

SegNet4D: Effective and Efficient 4D LiDAR Semantic Segmentation in Autonomous Driving Environments

Neng Wang*, Ruibin Guo*, Chenghao Shi, Hui Zhang, Huimin Lu[†], Zhiqiang Zheng, Xieyuanli Chen[†]

Abstract—4D LiDAR semantic segmentation, also referred to as multi-scan semantic segmentation, plays a crucial role in enhancing the environmental understanding capabilities of autonomous vehicles. It entails identifying the semantic category of each point in the LiDAR scan and distinguishing whether it is dynamic, a critical aspect in downstream tasks such as path planning and autonomous navigation. Existing methods for 4D semantic segmentation often rely on computationally intensive 4D convolutions for multi-scan input, resulting in poor real-time performance. In this article, we introduce SegNet4D, a novel real-time multi-scan semantic segmentation method leveraging a projection-based approach for fast motion feature encoding, showcasing outstanding performance. SegNet4D treats 4D semantic segmentation as two distinct tasks: single-scan semantic segmentation and moving object segmentation, each addressed by dedicated head. These results are then fused in the proposed motion-semantic fusion module to achieve comprehensive multi-scan semantic segmentation. Besides, we propose extracting instance information from the current scan and incorporating it into the network for instance-aware segmentation. Our approach exhibits state-of-the-art performance across multiple datasets and stands out as a real-time multi-scan semantic segmentation method. The implementation of SegNet4D will be made available at <https://github.com/nubot-nudt/SegNet4D>.

Index Terms—Autonomous driving, 4D semantic segmentation, deep learning, moving object segmentation.

I. INTRODUCTION

3D Light Detection and Ranging (LiDAR) sensor has become an indispensable device for modern autonomous vehicles and robots, attributed to its robustness to illumination variation and large field of view [1, 2]. Hence, LiDAR-based semantic perception has garnered extensive research interest in recent years. Semantic segmentation using 3D LiDAR data aims to assign a specific semantic class label to each point in the acquired point clouds, serving as a fundamental task in 3D perception. This process can significantly enhance downstream tasks, such as point cloud registration [3, 4] and simultaneous localization and mapping (SLAM) [5].

In practical applications, however, single-scan-based 3D LiDAR semantic segmentation methods [1, 6–8] are often applied restrictively as it lacks motion information, which significantly influences the continuous online processing for a same semantic object. To tackle this problem, the emerging field of 4D semantic perception has attracted increasing attention, focusing on categorizing each point and identifying its

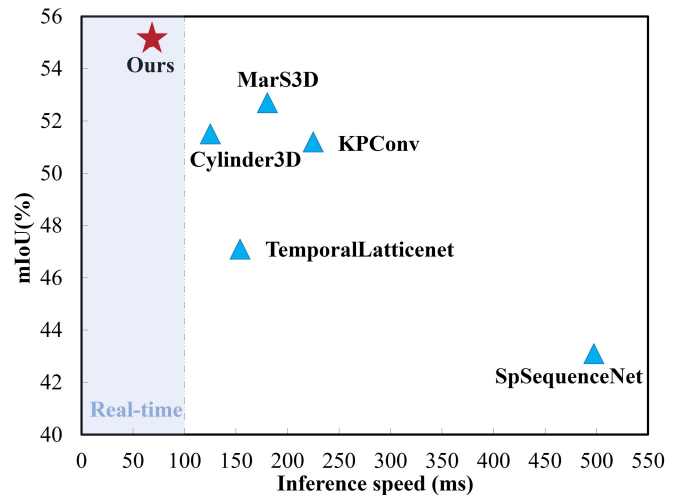


Fig. 1: Compared to existing methods, our SegNet4D achieves the best performance for multi-scan semantic segmentation on the SemanticKITTI benchmark while achieving real-time operation.

dynamic attributes simultaneously [9–11]. This task typically requires sequential multiple scans as input to extract motion information. In this regard, some methods directly stack historical LiDAR scans into a single pointcloud and feed it into a single-scan-based network for achieving multi-scan segmentation [1, 6, 7, 12], which lead to suboptimal performance due to the lack of temporal information association. Conversely, There are also methods exploring building 4D convolutional neural network [13] or recursive networks [10, 14] to extract motion features from input sequential LiDAR scans. However, these approaches impose heavy computational burdens and make real-time operation challenging. Besides, existing methods commonly treat multi-scan semantic segmentation in an end-to-end fashion, directly predicting semantic label for all categories. Due to the lower quantity of moving points in the scene compared to static points, this approach exhibits limited capability for recognizing moving objects.

To address these challenges, we propose an effective and efficient framework for multi-scan semantic segmentation. In our perspective, multi-scan semantic segmentation is a combination of single-scan semantic segmentation and moving object segmentation (MOS). Therefore, our key idea is to tackle multi-scan semantic segmentation by breaking it into two subtasks: single-scan semantic segmentation and MOS. By addressing each subtask with separate head and subsequently merging their results, our method achieves superior performance compared to the end-to-end manner. To enhance operational efficiency, our framework converts the sequential LiDAR scans into Bird’s Eye View (BEV) images and extracts

All authors are with the College of Intelligence Science and Technology, National University of Defense Technology, Changsha, China.

* Joint first authors with equal contribution.

[†] Joint corresponding authors: {lhmnew, xieyuanli.chen}@nudt.edu.cn

This work was supported in part by the National Science Foundation of China under Grant U22A2059, 62203460 and U1913202, as well as Major Project of Natural Science Foundation of Hunan Province under Grant 2021JC0004.

motion features by calculating BEV residuals, significantly reducing computational cost compared to existing methods using 4D convolutions. MOS [2, 15–20] is crucial for the final multi-scan semantics association, while existing methods cannot completely detect moving objects due to the lack of instance-level semantics. Therefore, we extract instance information from the current scan and integrate it into the prediction pipeline to improve MOS accuracy, enabling instance-aware segmentation. Finally, we design a novel module to fuse point-wise semantic predictions and motion states to achieve accurate multi-scan semantic segmentation online.

We extensively evaluate the proposed SegNet4D on mainstream datasets and compare its performance with other methods. As illustrated in Fig. 1, our approach achieves the best performance for multi-scan semantic segmentation tasks. To the best of our knowledge, this is the first real-time multi-scan semantic segmentation method with state-of-the-art performance. In addition, extensive experiments on multiple datasets also demonstrate that our network achieves state-of-the-art performance for the MOS task.

In sum, we make four key claims for this work:

- We propose a novel multi-scan semantic segmentation framework that decomposes this task into two subtasks, and finally merges their results to achieve more accurate segmentation.
- We propose an efficient multi-scan semantic segmentation network that is, to our best knowledge, the first method capable of real-time operation.
- We argue that instance information is beneficial for MOS and semantic segmentation tasks. So we incorporate instance information into the network to enable instance-aware segmentation.
- We design a novel motion-semantic fusion module for integrating motion predictions and single-scan semantic segmentation predictions, enabling the network to achieve motion-guided multi-scan segmentation.

II. RELATED WORK

A. Moving Object Segmentation.

MOS refers to accurately identifying dynamic regions or objects from input data. The task has attracted extensive research in the field of computer vision [21, 22]. In recent years, there has also been some research attention towards LiDAR-based MOS. We categorize these methods into projection-based and non-projection-based fashion.

The projection-based method typically converts sequential point clouds into image representations, such as range images [2, 15–17] or BEV images [18, 19], and then compute the residual of sequential images to extract motion information in the scene. Chen et al. [15] first released the MOS datasets and benchmark based on the SemanticKITTI dataset [12], and proposed a deep neural network to learn motion cues from sequential residual range images for online MOS. To extract motion features more comprehensively, Sun et al. [16] proposed a dual-branch network architecture that separately encodes the appearance features and temporal motion features,

and then fuses them with a multi-scale motion-guided attention module. Kim et al. [2] designed a similar multi-branch network, where one branch performs semantic segmentation to obtain movable objects, and another branch network extracts motion features. Finally, a fusion branch network is utilized to merge these features to achieve better MOS. Unlike range images, BEV images offer a top-down perspective that allows for a more intuitive observation of object movement. To boost the speeds of MOS, Mohapatra et al. [18] designed a lightweight network architecture for extracting motion information from BEV residual images and successfully achieved real-time operation in embedded GPU. However, this method can only perform pixel-wise segmentation in the BEV space and has relatively low accuracy. Recently, Zhou et al. [19] projected 3D point clouds into the polar coordinate BEV space and designed a dual-branch network structure similar to [16] to capture motion features and appearance features. Finally, these features are fused for effective MOS.

Different from the projection-based methods, the non-projection methods directly extract motion information from sequential 4D point clouds. Mersch et al. [20] utilized the Minkowski engine [13] to construct a sparse 4D convolutional network. This network is designed to extract spatio-temporal features from input 4D point clouds and predict point-wise moving labels. They also proposed a receding horizon strategy that integrates multiple observations to refine the network’s predictions. Kreutz et al. [23] proposed an unsupervised MOS method based on [20], which learns spatio-temporal occupancy changes in the local neighborhood of point cloud videos. However, it is only applicable to stationary LiDAR. Due to the lack of instance information, most MOS methods are unable to segment moving objects fully. Therefore, Wang et al. [24] introduced instance information into the MOS task and proposed a network capable of simultaneously detecting instances and moving objects, thereby integrating instance features and motion cues to achieve complete segmentation of moving objects.

B. 4D LiDAR Semantic Segmentation.

Unlike the MOS task, 4D LiDAR semantic segmentation requires additionally assigning a semantic category label to each point, including static and moving point. To address this task, some methods [1, 6, 7, 12] try to fuse sequential LiDAR scans into a single point cloud and then utilize a 3D semantic segmentation network to perform 4D semantic segmentation directly. However, due to the lack of temporal perception capability in 3D networks, these methods often show lower performance in semantic recognition for moving points. Moreover, the fused single point cloud has a large data volume, which greatly increases the computational workload of the network, making real-time operation challenging.

Another category of method builds temporal-aware networks to tackle multi-scan semantic segmentation task. SpSequenceNet [9] proposed two modules based on 3D convolutions, a cross-frame global attention module and a cross-frame local interpolation module, to extract spatio-temporal information from input 4D LiDAR scans. TemporalLidarSeg [10] recursively extracts features from the sequential point clouds

and utilizes a temporal memory alignment strategy to align the features of adjacent frames. Schutt et al. [14] proposed a recurrent architecture for fusing the features of continuous point clouds and designed a module for gathering temporal information. Recently, Liu et al. [11] proposed a module that converts the sequential point clouds into images and then utilizes a image network to extract motion features from the converted images. This module can provide the temporal awareness ability for existing 3D semantic segmentation networks.

However, these approaches still require extracting temporally related features from multiple point clouds, resulting in time-consuming for network operation. Unlike this, we separate the task of MOS and semantic segmentation, and finally utilize a motion-semantic fusion module to explicitly integrate motion predictions and semantic predictions, reducing the complexity of the task. Benefiting from quick motion feature extraction through projection fashion, our method can run in real-time.

III. OUR APPROACH

A. Our Framework

Given a sequential set of point clouds, we aim to obtain 4D semantic information for the current point cloud. To this end, we introduce SegNet4D. As shown in Fig. 2, SegNet4D consists of four main components: Motion Feature Encoding Module (MFEM), Instance Detection Module, Upsample Fusion Module, and Motion-Semantic Fusion Module (MSFM). The MFEM converts the current scan and the past consecutive scans into BEV images and subsequently computes the residuals of the BEV images to derive motion features. The Instance Detection Module then concatenates the motion features with the spatial features of the current LiDAR scan and extracts spatio-temporal features and instance features. These features are then fused in the Upsample Fusion Module. We utilize two separate output heads for the fused features to achieve single-scan semantic segmentation and MOS, respectively. Finally, the MSFM integrates single-scan semantic predictions and motion predictions, facilitating multi-scan semantic segmentation.

B. Motion Feature Encoding Module

A common way for motion feature extracting is 4D convolution [20, 23], which poses a significant computational workload. To improve the real-time performance, we adopt the BEV image representation for fast motion feature encoding through residual calculation. Initially, we perform spatial alignment by transforming past consecutive point clouds to the current viewpoint. Subsequently, we project the aligned point clouds into BEV images and compute the residuals between the current and the past consecutive BEV images. Moving objects will leave residual traces in the residual BEV image, as illustrated in Fig. 2. Finally, we back-project the BEV residual into 3D space as the motion features and subsequently concatenate them with the current point cloud as input of the network.

Point Cloud Alignment. Given the current point cloud $\mathcal{S}_0 = \{\mathbf{p}_i \in \mathbb{R}^4\}_{i=1}^M$ consisting of M points represented in

homogeneous coordinates as $\mathbf{p}_i = [x_i, y_i, z_i, 1]^\top$, along with the past $N - 1$ consecutive point clouds $\mathcal{S}_1, \mathcal{S}_2, \dots, \mathcal{S}_{N-1}$ with their transformations $\mathbf{T}_1^0, \mathbf{T}_2^1, \dots, \mathbf{T}_{N-1}^{N-1}$ relative to \mathcal{S}_0 , we transform the past $N - 1$ consecutive point clouds into the current viewpoint by

$$\mathcal{S}_{j \rightarrow 0} = \{\mathbf{p}'_i = \mathbf{T}_j^0 \mathbf{p}_i | \mathbf{p}_i \in \mathcal{S}_j\}, \quad \mathbf{T}_j^0 = \prod_{k=0}^{j-1} \mathbf{T}_{j-k}^{j-k-1}. \quad (1)$$

In practice, the relative pose transformations can be easily obtained through the existing LiDAR SLAM approach, e.g., SuMa [5].

BEV Projection. After alignment, we project the aligned point clouds into single-channel BEV images. For each point $\mathbf{p}'_j = (x'_j, y'_j, z'_j) \in \mathcal{S}_{j \rightarrow 0}$, we first restrict it within $x'_j \in [X_{min}, X_{max}]$, $y'_j \in [Y_{min}, Y_{max}]$, $z'_j \in [Z_{min}, Z_{max}]$ and then reconvert it into the pillar space, given by

$$\begin{cases} I_{(u,v),j} = \{z'_j | z'_j \in \mathbf{p}'_j\}, \\ u = \lfloor \frac{x'_j - X_{min}}{g} \rfloor, \\ v = \lfloor \frac{y'_j - Y_{min}}{g} \rfloor, \end{cases} \quad (2)$$

where $I_{(u,v),j}$ represents the height of the point in $\mathcal{S}_{j \rightarrow 0}$ located at (u, v) pillar and g denotes grid resolution.

Following [19], we project the I_j into a single-channel BEV image \mathcal{B}_j of size $H \times W$. For each pixel value $\mathcal{B}_{(u,v),j}$, we use the difference between the maximum and minimum height within the same pillar, calculating as:

$$\mathcal{B}_{(u,v),j} = \text{Max}\{I_{(u,v),j}\} - \text{Min}\{I_{(u,v),j}\} \quad (3)$$

Motion Features Extraction. We take the BEV residuals $\mathcal{R} \in \mathbb{R}^{H \times W \times (N-1)}$ between \mathcal{B}_0 and $\mathcal{B}_1, \dots, \mathcal{B}_{N-1}$ as the motion features in the BEV space, calculated by

$$\mathcal{R}_{(u,v),j \rightarrow 0} = \mathcal{B}_{(u,v),0} - \mathcal{B}_{(u,v),j}, j \in 1, \dots, N-1, \quad (4)$$

where $\mathcal{R}_{(u,v)}$ represents the residual value for pixel at (u, v) . To obtain motion features for each point in the 3D space, we perform back-projection by assigning the BEV residual value to all points projected to the BEV pixel. Points within the same pillar will share the same residual value. Finally, we obtain point-wise motion features $\mathcal{F}_m \in \mathbb{R}^{M \times (N-1)}$.

C. Instance Detection Module

For tasks such as MOS or semantic segmentation, instance often cannot be further segmented. Segmenting an instance into different parts is a typical result of incorrect segmentation. Similar to human perception, when identifying moving objects, they first determine whether the object is moving and then reason the points on it are also moving. This instance-aware reasoning process can alleviate a common issue in existing MOS methods: distinct parts of a single object can be erroneously classified as different labels. Inspired by this, we design the Instance Detection Module to detect instances and incorporate them into our network.

We concatenate spatial coordinates $\mathcal{S}_0 \in \mathbb{R}^{M \times 4}$ and the motion features \mathcal{F}_m of the current scan and obtain the new features $\mathcal{F}_{sp} \in \mathbb{R}^{M \times (N+3)}$ as the input. We use 3D sparse convolution blocks [25] to first voxelize the current point cloud and then perform convolution only on non-empty voxels,

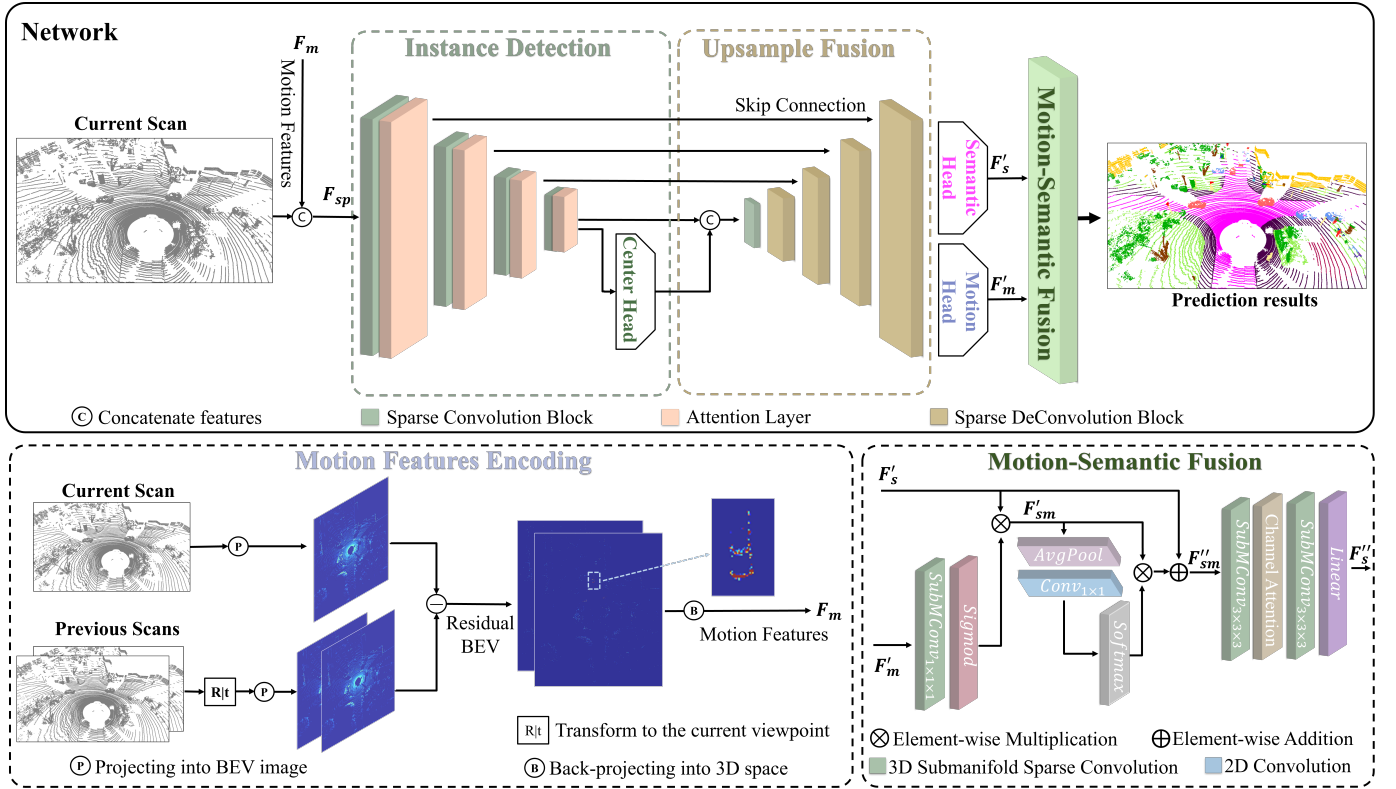


Fig. 2: The proposed framework of SegNet4D. The Motion Features Encoding Module converts the sequential LiDAR scans into BEV images for residual calculation and then extract motion features from the residual images. Following this, the motion features are concatenated with the spatial features of the current scan and fed into the Instance Detection Module to extract instance features. These instance features are further fused in the Upsample Fusion Module, after which a semantic head is utilized to predict confidence scores for semantic categories, and a motion head to predict moving confidence scores. Ultimately, the Motion-Semantic Fusion Module integrates semantic categories and motion states to achieve multi-scan semantic segmentation.

greatly improving the processing speed. Moreover, in order to capture more crucial features, we add a window self-attention [26] layer after each sparse convolution block to improve the receptive field. Finally, we utilize CenterHead [27] to predict instance information of the current scan. The CenterHead main comprises two output heads: one head generates multiple heatmaps for predicting the category and center positions of instances, while the other head is used to estimate the bounding box of the instances.

D. Upsample Fusion Module

The Upsample Fusion Module serves the main purpose of integrating instance features into the prediction pipeline, as well as recovering the scale of the features hierarchically through 3D deconvolution blocks. It is formed by a complete U-Net network structure together with the Instance Detection Module and maintains more details from different scale features through skip connection. Incorporating instance information into the prediction process enables the network to achieve instance-aware segmentation. However, to reduce the network's computational cost, we introduce instance features at the smallest spatial scale.

E. Output Head

To maintain the network's lightweight characteristics, we directly utilize two distinct output heads to achieve single-scan semantic segmentation and MOS simultaneously. The

output head consists of convolutional layers and linear layers, which are employed to further classify features with different attributes. Finally, we can obtain point-wise semantic features $F'_s \in \mathbb{R}^{M \times C}$ and motion features $F'_m \in \mathbb{R}^{M \times 3}$. By applying the softmax function, the network can output the semantic labels and motion labels of the current point cloud. Note that 3 represents three different motion properties, namely unlabeled, static, and moving, while C denotes the number of semantic categories. We set $C = 20$ in the SemanticKITTI dataset and $C = 17$ in the nuScenes dataset.

F. Motion-Semantic Fusion Module

To achieve multi-scan semantic segmentation, one direct way is to manually fuse motion labels and static semantic labels. However, this can result in non-smooth point segmentation. Moreover, incorrect motion predictions directly lead to false multi-scan semantic segmentation. We hence propose the MSFM to integrate motion features F'_m and static semantic features F'_s for achieving motion-guided multi-scan semantic segmentation. Details of this module are illustrated in Fig. 2.

We build our Motion-Semantic Fusion Module upon recently advanced motion-guided attention module [28] in the field of image processing. We utilize the 3D submanifold sparse convolution [25] as the backbone for performing spatial attention and fusing F'_s with F'_m as:

$$F'_{sm} = F'_s \otimes \text{Sigmoid}(\text{SubMConv}_{1 \times 1 \times 1}(F'_m)), \quad (5)$$

where \otimes represent element-wise multiplication, $\text{SubMConv}_{1 \times 1 \times 1}(\cdot)$ represent a 3D submanifold sparse convolution with $1 \times 1 \times 1$ kernel size, and $\mathbf{F}'_{sm} \in \mathbb{R}^{M \times D}$ are the fused motion-salient features, and D denotes the number of feature channels. We then perform channel attention for \mathbf{F}'_{sm} to strengthen the responses of key attributes, which is then element-wisely added by \mathbf{F}'_s as the static semantic features is equally crucial for the multi-scan semantic segmentation. The final \mathbf{F}''_{sm} is written as:

$$\mathbf{F}''_{sm} = \mathbf{F}'_{sm} \otimes [\text{Softmax}(\text{Conv}_{1 \times 1}(\text{AvgPool}(\mathbf{F}'_{sm}))) \cdot D] + \mathbf{F}'_s, \quad (6)$$

where $\text{Conv}_{1 \times 1}(\cdot)$ and $\text{AvgPool}(\cdot)$ denote a 2D convolution with 1×1 kernel size and average pooling operation, respectively. 2D convolution is mainly used to quickly calculate channel attention weights, which is different from using 3D convolution for spatial attention as mentioned earlier.

Finally, we further refine \mathbf{F}''_{sm} using 3D sparse convolutions and channel attention blocks [29] to generate the final multi-scan semantic segmentation predictions $\mathbf{F}''_s \in \mathbb{R}^{M \times C'}$, where C' is the number of categories for multi-scan semantic segmentation.

G. Moving Instance Refinement

The network can output moving instances by directly checking the predicted MOS label of the instance center point. However, relying solely on this bottom-up fashion may lead to false detection, thus enlarging the amount of misclassified points. To further enhance MOS performance, we check again the point-wise predictions within an instance and propose an instance-based refinement algorithm in a combined bottom-up and top-down fashion.

The key ideas of this refinement algorithm can be summarized as follows: Firstly, if many points within an instance are moving, then the instance is considered to be moving. Conversely, all points within moving instances are classified as moving. Secondly, if the scene contains many moving vehicles, it is categorized as a highly dynamic scene, such as the highway. Vehicles in this scene will be more easily classified as moving class with a lower confidence threshold. Finally, because motion is a continuous process, we consider an instance to be moving only when it is classified as moving class in multiple observations.

H. Loss Function

Due to multi-task setup, our loss function includes instance detection loss L_{det} , moving object segmentation loss L_{mos} , single-scan semantic segmentation loss $L_{\text{s_sem}}$ and multi-scan semantic segmentation loss $L_{\text{m_sem}}$. In order to achieve a balance between the magnitudes of different loss functions and to expedite the convergence speed, we apply a weighted multi-task loss [30] L_{total} to supervise the training, defined as:

$$L_{\text{total}} = \sum_{i \in \{\text{det, mos, s_sem, m_sem}\}} \frac{1}{2\sigma_i^2} L_i + \ln(1 + \sigma_i^2), \quad (7)$$

where σ_i is a learnable parameter used to represent the uncertainty of L_i . L_{det} is composed of instance classification loss and bounding box regression loss, which is defined in [24]. In

addition, we employ the widely used weighed Cross-Entropy Loss function [16] for L_{mos} , $L_{\text{s_sem}}$ and $L_{\text{m_sem}}$:

$$L_{\{\text{mos, s_sem, m_sem}\}}(y, \hat{y}) = -\sum \alpha_i p(y_i) \log(p(\hat{y}_i)), \alpha_i = 1/\sqrt{f_i}, \quad (8)$$

where y_i and \hat{y}_i denote the ground truth and the predicted labels, respectively. f_i is the frequency of the i -th class.

IV. EXPERIMENTAL EVALUATION

In this section, we conduct a series of experiments on multi-datasets to demonstrate the performance of our method for multi-scan semantic segmentation, single-scan semantic segmentation, and MOS. We compare the performance with state-of-the-art both quantitatively and qualitatively. Additionally, we perform ablation experiments on our network to evaluate the effectiveness of our framework and the proposed modules. These experimental results will substantiate our claims.

A. Experimental setup

Datasets-SemanticKITTI. SemanticKITTI [12] is widely used for outdoor point cloud segmentation tasks, including MOS and semantic segmentation. It consists of 22 sequences collected with Velodyne HDL-64E LiDAR, splitting sequences 00-07, 09-10 as the training set, sequence 08 as the validation set, and sequences 11-21 as the test set. The dataset contains multiple semantic category labels. In our model, the training is supervised with 26 semantic categories, including 6 moving classes, 19 static classes, and one *outlier* class. Moreover, we utilize the L-Shape method [31] to refine the object bounding box proposed in InsMOS[24]. For the MOS task, we follow previous works and reorganize all the semantic categories into two classes: moving and static. Due to the imbalanced distribution of moving objects between the training set and the test set, an additional dataset, KITTI-Road, is introduced in [16] to mitigate the impact. Following the experimental setups described in [16], we train an additional model using the extended dataset. For a fair comparison, we report both the MOS evaluation results using only the SemanticKITTI dataset and the extended KITTI-Road dataset.

Datasets-nuScenes. It consists of 1000 driving scenes collected with a 32-beam LiDAR sensor. Each scene lasts for 20 seconds and is sampled at a frequency of 20 Hz. For point cloud segmentation tasks, it is mainly used for evaluating static semantic segmentation with 16 semantic classes. To achieve multi-scan segmentation, we utilize the annotated bounding box attributes to generate 8 new moving semantic categories, including moving car, bus, truck, construction vehicle, trailer, motorcyclist, bicyclist, and person. We will release the multi-scan semantic segmentation dataset of nuScenes for the convenience of the community. Similar to the SemanticKITTI, we divide all semantic categories into two classes (moving and static) for evaluating MOS. Since the labels of test set are not available, we only use the nuScenes validation set to evaluate the MOS and multi-scan semantic segmentation performance.

Dataset-SipailouCampus. It is proposed in [19] for MOS evaluation. Different from the SemanticKITTI and nuScenes, it collects the data with a solid-state LiDAR for evaluating

TABLE I: Multi-scan semantic segmentation performance evaluation on the SemanticKITTI hidden test set. “mov.” denotes moving category. The best results are in bold.

| Methods | car | bicycle | motorcycle | truck | other-vehicle | person | bicyclist | motorcyclist | road | parking | sidewalk | other-ground | building | fence | vegetation | trunk | terrain | pole | traffic sign | mov. car | mov. truck | mov. other veh. | mov. person | mov. bicyclist | mov. motorcycle | mIoU |
|-------------|-------------|-------------|-------------|-------------|---------------|-------------|------------|--------------|-------------|-------------|-------------|--------------|-------------|-------------|-------------|-------------|-------------|-------------|--------------|-------------|-------------|-----------------|-------------|----------------|-----------------|-------------|
| TangentConv | 84.9 | 2.0 | 18.2 | 21.1 | 18.5 | 1.6 | 0.0 | 0.0 | 83.9 | 38.3 | 64.0 | 15.3 | 85.8 | 49.1 | 79.5 | 43.2 | 56.7 | 36.4 | 31.2 | 40.3 | 1.1 | 6.4 | 1.9 | 30.1 | 42.2 | 34.1 |
| DarkNet53 | 84.1 | 30.4 | 32.9 | 20.0 | 20.7 | 7.5 | 0.0 | 0.0 | 91.6 | 64.9 | 75.3 | 27.5 | 85.2 | 56.5 | 78.4 | 50.7 | 64.8 | 38.1 | 53.3 | 61.5 | 14.1 | 15.2 | 0.2 | 28.9 | 37.8 | 41.6 |
| SSN | 88.5 | 24.0 | 26.2 | 29.2 | 22.7 | 6.3 | 0.0 | 0.0 | 90.1 | 57.6 | 73.9 | 27.1 | 91.2 | 66.8 | 84.0 | 66.0 | 65.7 | 50.8 | 48.7 | 53.2 | 41.2 | 26.2 | 36.2 | 2.3 | 0.1 | 43.1 |
| TLS | 92.1 | 47.7 | 40.9 | 39.2 | 35.0 | 14.4 | 0.0 | 0.0 | 91.8 | 59.6 | 75.8 | 23.2 | 89.8 | 63.8 | 82.3 | 62.5 | 64.7 | 52.6 | 60.4 | 68.2 | 2.1 | 12.4 | 40.4 | 42.8 | 12.9 | 47.0 |
| TLN | 91.6 | 35.4 | 36.1 | 26.9 | 23.0 | 9.4 | 0.0 | 0.0 | 91.5 | 59.3 | 75.3 | 27.5 | 89.6 | 65.3 | 84.6 | 66.7 | 70.4 | 57.2 | 60.4 | 59.7 | 0.0 | 5.9 | 51.0 | 41.7 | 48.8 | 47.1 |
| KPCConv | 93.7 | 44.9 | 47.2 | 42.5 | 38.6 | 21.6 | 0.0 | 0.0 | 86.5 | 58.4 | 70.5 | 26.7 | 90.8 | 64.5 | 84.6 | 70.3 | 66.0 | 57.0 | 53.9 | 69.4 | 0.5 | 0.5 | 67.5 | 67.4 | 47.2 | 51.2 |
| Cylinder3D | 93.8 | 67.6 | 63.3 | 41.2 | 37.6 | 12.9 | 0.1 | 0.1 | 90.4 | 66.3 | 74.9 | 32.1 | 92.4 | 65.8 | 85.4 | 72.8 | 68.1 | 62.6 | 61.3 | 68.1 | 0.0 | 0.1 | 63.1 | 60.0 | 0.4 | 51.5 |
| MarS3D | 95.1 | 49.2 | 49.5 | 39.7 | 36.6 | 16.2 | 1.2 | 0.0 | 89.9 | 66.8 | 74.3 | 26.4 | 92.1 | 68.2 | 86.0 | 72.1 | 70.5 | 62.8 | 64.8 | 78.4 | 5.1 | 10.0 | 58.0 | 67.3 | 36.3 | 52.7 |
| Ours | 94.6 | 49.4 | 49.3 | 35.7 | 42.1 | 9.3 | 0.0 | 14.0 | 92.1 | 65.2 | 76.7 | 29.6 | 92.2 | 69.1 | 84.9 | 70.0 | 68.3 | 59.1 | 63.6 | 78.2 | 3.6 | 37.6 | 55.9 | 71.5 | 62.4 | 55.0 |

the effectiveness of the MOS method across different types of LiDAR sensors. It contains 7 sequences with only moving and static labels, divided into 5 sequences for training, 1 sequence for validation, and 2 sequences for testing. We follow the experimental setups in [19] to evaluate MOS performance and compare the result with other methods.

Implementation Details. We restrict the point cloud range in $[x : \pm 60m, y : \pm 50m, z : -4m \sim 2m]$ for SemanticKITTI and SipailouCampus, $[x : \pm 50m, y : \pm 50m, z : -4m \sim 2m]$ for nuScenes, and set $g = 0.1m$ for encoding motion features. For multi-scan semantic segmentation, we set $C = 20$, $C' = 26$ for SemanticKITTI and $C = 17$, $C' = 25$ for nuScenes. The proposed model is built on the PyTorch [32] library and trained with 4 NVIDIA RTX 3090 GPUs. We set the batch size to 8 on a single GPU. During the training process, we employ data augmentation techniques such as random flipping, scaling, and rotation to improve model performance.

Evaluation Metrics. For MOS performance evaluation, we use the Intersection-over-Union (IoU) [33] of moving objects as the metric:

$$\text{IoU} = \frac{\text{TP}}{\text{TP} + \text{FP} + \text{FN}}, \quad (9)$$

where TP, FP, and FN represent the predictions of the moving class that are classified as true positive, false positive, and false negative, respectively. For semantic segmentation, we use the mean Intersection-over-Union (mIoU) across all categories as the evaluation metric.

B. Main Results

Multi-scan Semantic Segmentation. We evaluate the multi-scan semantic segmentation performance of our approach on the SemanticKITTI hidden test set and compare the results with baseline methods, including (a) single-scan-based methods (stack historical LiDAR scans into a single scan as input for multi-scans semantic segmentation): TangentConv[7], DarkNet53[12], KPCConv[6], Cylinder3D[1]; and specially designed multi-scans-based semantic segmentation methods: SpSequenceNet (SSN) [9], TemporalLidarSeg (TLS) [10],

TemporalLatticeNet (TLN) [14], MarS3D[11]. Like all methods, we only utilize the past two LiDAR scans to predict semantic labels for a fair comparison, i.e., $N = 3$.

As shown in Tab. I, our approach achieves a mIoU of 55.0% without using any test-time augmentation and multi-model ensemble tricks, and the performance outperforms all methods. In particular, our method demonstrates significant improvements in semantic recognition of moving objects compared to other approaches.

To further test the adaptability of our method to a sparser point cloud, we conduct additional experiments on the nuScenes dataset and compare the results with latest method: MarS3D. From the results presented in Tab. II, our method operates well on sparser point cloud data, and the performance is still superior to MarS3D. We also qualitatively compare our approach with MarS3D on the nuScenes validation set, as shown in Fig. 3. Our approach shows better semantic recognition capabilities for moving objects. Additionally, MarS3D tends to incorrectly classify big instances, such as trucks. It often exhibits incomplete segmentation.

Single-scan Semantic Segmentation. We report the single-scan semantic segmentation results of our method on the SemanticKITTI hidden test set and compare them with the single-scan-based method in Tab. I, as shown in Tab. III. Although our method does not achieve the best performance for single-scan semantic segmentation, it still gets competitive results.

Moving Object Segmentation. We evaluate the results on the SemanticKITTI-MOS benchmark and compare the performance with several MOS methods, including (a) projection-based methods: LMNet [17], RVMOS [2], MotionSeg3D [16], and MotionBEV [19]; (b) point-based methods: 4DMOS [20] and InsMOS [24]; and (c) an offline method: AutoMOS [17]. SemanticKITTI-MOS benchmark is an official MOS evaluator proposed in [17], which contains data and labels of the SemanticKITTI hidden test set. Note that the experimental results of these methods are derived from their original paper and SemanticKITTI-MOS benchmark. In particular, to achieve

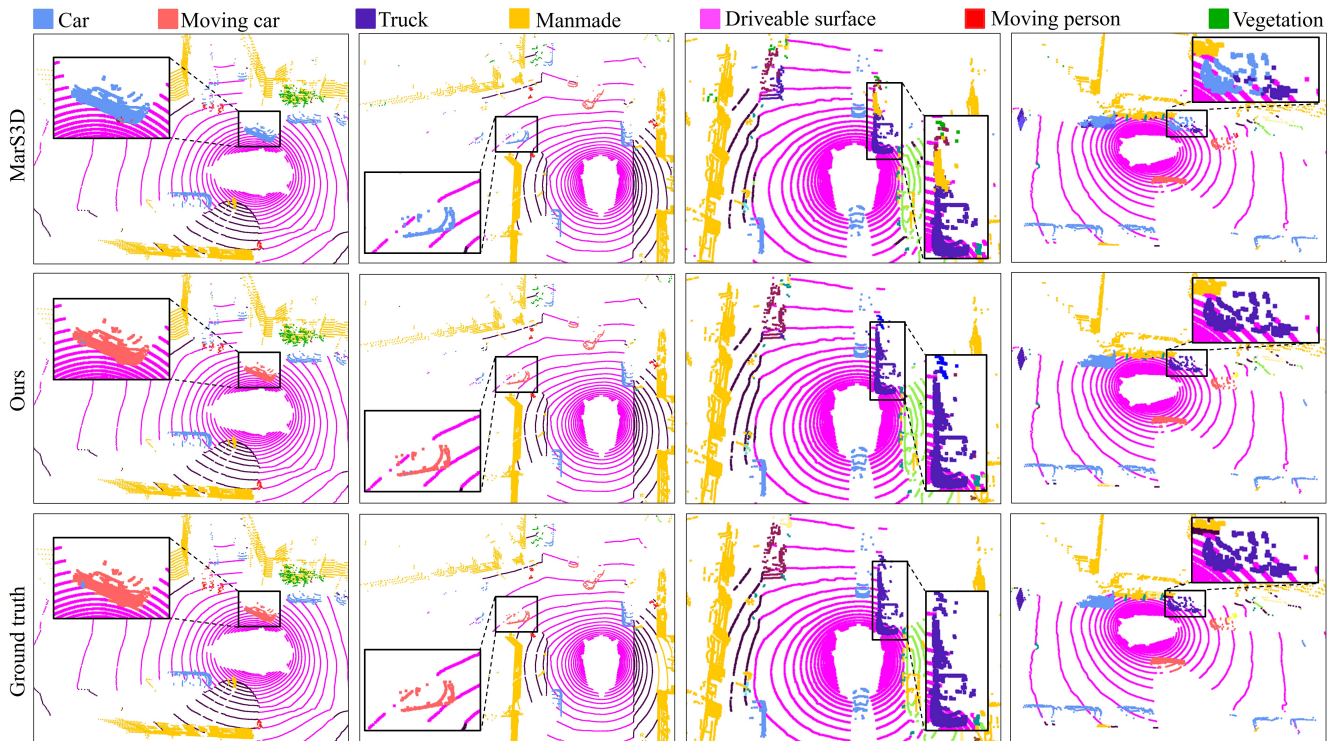


Fig. 3: The qualitative visualization results comparison between our approach and MarS3D on the nuScenes validation set.

TABLE II: Multi-scan semantic segmentation performance evaluation on the nuScenes validation set. “mov.” denotes moving category. The best results are in bold.

| Methods | barrier | bicycle | bus | car | construction | motorcycle | pedestrian | traffic cone | trailer | truck | driveable | other flat | sidewalk | terrain | manmade | vegetation | mov. car | mov. bus | mov. truck | mov. const. | mov. trailer | mov. motor. | mov. bicyc. | mov. person | mIoU |
|---------|-------------|-------------|-------------|-------------|--------------|-------------|-------------|--------------|-------------|-------------|-------------|-------------|-------------|-------------|-------------|-------------|-------------|-------------|-------------|-------------|--------------|-------------|-------------|-------------|-------------|
| MarS3D | 70.5 | 24.7 | 60.0 | 79.9 | 32.0 | 34.9 | 51.3 | 53.0 | 10.4 | 66.0 | 95.4 | 59.9 | 72.7 | 75.8 | 87.2 | 86.1 | 66.5 | 48.0 | 52.4 | 0.0 | 23.1 | 69.0 | 9.7 | 72.7 | 54.3 |
| Ours | 77.4 | 32.6 | 63.8 | 73.8 | 41.1 | 44.0 | 51.2 | 63.2 | 42.3 | 74.2 | 96.2 | 69.3 | 74.2 | 73.5 | 64.6 | 55.9 | 68.6 | 51.3 | 59.4 | 0.0 | 27.2 | 74.3 | 40.8 | 72.4 | 57.9 |

TABLE III: Single-scan semantic segmentation performance evaluation on the SemanticKITTI hidden test set. The best results are in bold.

| Methods | mIoU[%] |
|-------------|-------------|
| TangentConv | 35.9 |
| Darknet53 | 49.9 |
| KPConv | 58.8 |
| Cylinder3D | 67.8 |
| Ours | 65.2 |

the best MOS performance, we set $N = 8$ for the MOS task.

We present quantitative comparison in Tab. IV. Without using the KITTI-Road dataset for training, our method performs only worse than RVMOS on the SemanticKITTI test set, but is significantly better than other methods. By utilizing the extended dataset to mitigate the influence of imbalanced data distribution, our approach achieves the best performance of 77.5% IoU.

To further compare the performance of all methods, we conduct additional experiments on the SipailouCampus and nuScenes dataset, as depicted in Tab. V. Note that we apply

TABLE IV: MOS performance comparison on the SemanticKITTI-MOS benchmark. The best results are in bold.

| Methods | +Road | IoU[%] |
|-------------|-------|-------------|
| LMNet | | 62.5 |
| 4DMOS | | 65.2 |
| RVMOS | | 74.7 |
| MotionBEV | | 69.7 |
| AutoMOS | ✓ | 62.3 |
| MotionSeg3D | ✓ | 70.2 |
| InsMOS | ✓ | 75.6 |
| Ours | | 71.9 |
| Ours | ✓ | 77.5 |

the same pose transformations to all methods for fairness. Due to RVMOS not being open source, we are unable to evaluate its performance on the additional datasets. However, from the results of the SemanticKITTI validation set, our approach significantly outperforms it. Meanwhile, our approach also demonstrates the best performance across multiple datasets collected by different types of LiDAR sensors.

In addition, we also qualitatively compare our results with the latest MOS methods: InsMOS and MotionBEV. As illus-

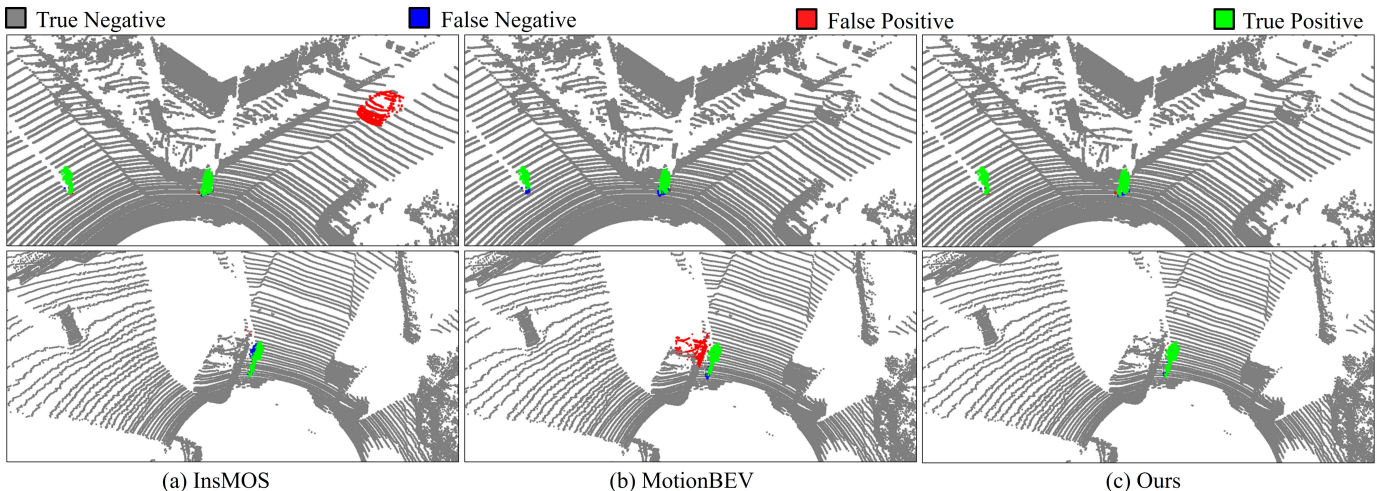


Fig. 4: The qualitative results comparison with InsMOS and MotionBEV on SemanticKITTI validation set. Best viewed in color.

TABLE V: Comparing the IoU[%] of moving objects on multiple datasets. The best results are in bold.

| Methods | SemanticKITTI validation | Sipailou Campus | nuScenes validation |
|-------------|--------------------------|-----------------|---------------------|
| LMNet | 67.1 | 56.2 | 49.9 |
| 4DMOS | 71.9 | 88.9 | 67.8 |
| RVMOS | 71.2 | - | - |
| MotionBEV | 76.5 | 90.8 | 64.7 |
| MotionSeg3D | 71.4 | 66.8 | 63.0 |
| InsMOS | 73.2 | 90.0 | 65.7 |
| Ours | 77.6 | 91.3 | 69.0 |

trated in Fig. 4, although InsMOS is able to completely segment moving objects by incorporating instance information, there are occasional cases where it completely missegments an object due to the insufficient motion perception capability of the backbone. Similarly, MotionBEV exhibits subpar performance under circumstances where moving objects are in close proximity to static objects. In comparison, our method can segment moving objects accurately in various scenarios.

C. Ablation Study

Our method separately predicts moving objects and single-scan semantic labels, and finally feeds them into the MSFM module to achieve multi-scan semantic segmentation. Therefore, accurate motion predictions can improve the performance of multi-scan segmentation. Based on this, we first conduct studies on BEV residual images grid resolution g in the motion features extraction process to obtain optimal MOS performance. Subsequently, we conduct ablation experiments on our framework and MSFM module to test their effectiveness.

The results of different numbers of g on the MOS task are presented in Tab. VI. As can be seen, when g decreases, our approach performs much better because the MFEM can capture more detailed features. However, a smaller grid resolution will increase the time required for motion feature extraction, so we select $g = 0.1$ to achieve a good balance between computational complexity and accuracy.

TABLE VI: Comparing the IoU[%] of different g on the SemanticKITTI validation set for MOS task.

| g | 0.05m | 0.1m | 0.2m | 0.3m |
|--------|-------|------|------|------|
| IoU[%] | 78.0 | 77.6 | 76.1 | 75.8 |

TABLE VII: The network ablation studies on the nuScenes dataset. **MOS**: moving object segmentation. **Single Sem**: single-scan semantic segmentation. **Multi Sem**: multi-scan semantic segmentation. Metric: the IoU of moving objects for MOS, mIoU for Single Sem and Multi Sem.

| | Inst- ance | One Head | Two Head | Refin- ement | MOS | Single Sem | Multi Sem |
|-----|---------------|-------------|-------------|-----------------|------|---------------|--------------|
| [A] | | | ✓ | | 67.1 | 67.3 | 55.5 |
| [B] | ✓ | ✓ | | | - | - | 56.0 |
| [C] | ✓ | | ✓ | | 68.5 | 68.6 | 57.4 |
| [D] | ✓ | | ✓ | ✓ | 69.0 | 68.6 | 57.5 |

In Tab. VII, we train different models to test the effectiveness of our network components. Here, “Instance” indicates whether instance information is integrated into the Upsample Fusion Module to achieve instance-aware segmentation. “One Head” means directly predicting multi-scan semantic labels using only one multi-scan semantic head. “Two Head” means utilizing two heads (a semantic head and a motion head) to predict single-scan semantic labels and moving objects, respectively, and finally merging their results to achieve multi-scan semantic segmentation. “Refinement” refers to moving instance refinement mentioned in Section III-G, and it only focuses on refining the prediction of moving objects. Note that the multi-scan semantic segmentation results are generated by manually merging MOS and single-scan semantic predictions. By comparing model [A] and [C], we can see that incorporating instance information can improve the accuracy of MOS and semantic segmentation, thus substantiating our third claim. The comparison between model [B] and [C] shows the effectiveness of decomposing the complex multi-scan semantic segmentation task into two subtasks. Furthermore, this framework demonstrates superior performance in comparison to directly

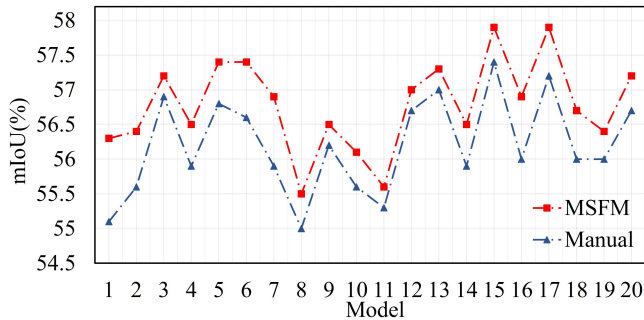


Fig. 5: Ablation study. Comparing the results of MSFM and manual fusion for 20 stabilized models on nuScenes validation set.

predicting multi-scan semantic labels in an end-to-end manner, which supports our first claim. The results of model [C] and [D] indicate that the refinement is effective for refining the predictions of MOS. And the refinement of MOS predictions can improve the results of multi-scan semantic segmentation.

Finally, to verify the effectiveness of the MSFM module, we manually merge the predictions of MOS and single-scan semantic segmentation as multi-scan semantic segmentation results, represented as Manual. And compare it with the segmentation results of the MSFM module, as shown in Fig. 5. To mitigate the potential randomness of single statistic, we record 20 models that become stable during the training process for comparing the results. It can be seen that the MSFM module always outperforms manual fusion, which proves its effectiveness in integrating motion and semantic prediction. The results also demonstrate our fourth claim.

D. Runtime

We provide a detailed runtime comparison for multi-scan semantic segmentation in Tab. VIII. We test the average time on the SemanticKITTI validation set using a single NVIDIA RTX 3090 GPU. Specifically, since we can not reproduce the results of KPConv multi-scan segmentation and TemporalLatticenet on our machine, we acquire their runtime from [14], and they are tested using the same GPU. From the results, the existing methods all have a runtime time exceeding 100ms, rendering them unsuitable for real-time operation. In contrast, our method achieves a runtime time of 67.1ms and is the sole approach capable of real-time operation, which proves that our method is efficient for 4D LiDAR semantic segmentation. These results support our second claim.

V. CONCLUSION

In this paper, we present a novel multi-scan semantic segmentation method to predict both point-wise moving labels and semantic labels for LiDAR data, and operate in real-time. The framework decomposes the complex multi-scan semantic segmentation task into single-scan semantic segmentation and MOS tasks, finally merging their prediction to achieve more accurate multi-scan semantic segmentation. We adopt a projection-based approach to quickly obtain motion features, which significantly reduces the computational complexity compared to 4D convolutions. To achieve instance-aware segmentation, we concatenate the motion features with the spatial features of the current scan, feeding them into the

TABLE VIII: Comparing the runtime of multi-scan semantic segmentation methods. The fastest runtime is in bold.

| Methods | Runtime[ms] |
|--------------------|-------------|
| SpSequenceNet | 497.3 |
| KPConv | 225.0 |
| TemporalLatticenet | 154.0 |
| Cylinder3D | 125.0 |
| MarS3D | 180.5 |
| Ours | 67.1 |

network for instance detection, and subsequently inject the instance features into the prediction pipeline. In addition, we design a motion-semantic fusion module to explicitly integrate the point-wise motion states and static semantic predictions, enabling motion-guided multi-scan semantic segmentation. Extensive experiments on multiple datasets demonstrate that our approach is effective and efficient.

REFERENCES

- [1] X. Zhu, H. Zhou, T. Wang, F. Hong, W. Li, Y. Ma, H. Li, R. Yang, and D. Lin, "Cylindrical and asymmetrical 3d convolution networks for lidar-based perception," *IEEE Trans. on Pattern Analysis and Machine Intelligence (TPAMI)*, vol. 44, no. 10, pp. 6807–6822, 2022.
- [2] J. Kim, J. Woo, and S. Im, "Rvmos: Range-view moving object segmentation leveraged by semantic and motion features," *IEEE Robotics and Automation Letters (RA-L)*, vol. 7, no. 3, pp. 8044–8051, 2022.
- [3] W. Lu, G. Wan, Y. Zhou, X. Fu, P. Yuan, and S. Song, "Deepvcv: An end-to-end deep neural network for point cloud registration," in *Proc. of the IEEE/CVF Intl. Conf. on Computer Vision (ICCV)*, 2019, pp. 12–21.
- [4] C. Shi, X. Chen, H. Lu, W. Deng, J. Xiao, and B. Dai, "Rdmnet: Reliable dense matching based point cloud registration for autonomous driving," *IEEE Trans. on Intelligent Transportation Systems (ITS)*, vol. 24, no. 10, pp. 11 372–11 383, 2023.
- [5] J. Behley and C. Stachniss, "Efficient Surfel-Based SLAM using 3D Laser Range Data in Urban Environments," in *Proc. of Robotics: Science and Systems (RSS)*, 2018.
- [6] H. Thomas, C. R. Qi, J. Deschaud, B. Marcotegui, F. Goulette, and L. J. Guibas, "KPConv: Flexible and Deformable Convolution for Point Clouds," in *Proc. of the IEEE/CVF Intl. Conf. on Computer Vision (ICCV)*, 2019.
- [7] M. Tatarchenko, J. Park, V. Koltun, and Q.-Y. Zhou, "Tangent Convolutions for Dense Prediction in 3D," in *Proc. of the IEEE Conf. on Computer Vision and Pattern Recognition (CVPR)*, 2018.
- [8] S. Li, X. Chen, Y. Liu, D. Dai, C. Stachniss, and J. Gall, "Multi-scale Interaction for Real-time LiDAR Data Segmentation on an Embedded Platform," *IEEE Robotics and Automation Letters (RA-L)*, vol. 7, no. 2, pp. 738–745, 2022.
- [9] H. Shi, G. Lin, H. Wang, T. Y. Hung, and Z. Wang, "SpSequenceNet: Semantic Segmentation Network on 4D Point Clouds," in *Proc. of the IEEE/CVF Conf. on Computer Vision and Pattern Recognition (CVPR)*, 2020.
- [10] F. Duerr, M. Pfaller, H. Weigel, and J. Beyerer, "Lidar-based recurrent 3d semantic segmentation with temporal memory alignment," *Proc. of the Intl. Conf. on 3D Vision (3DV)*, pp. 781–790, 2020.
- [11] J. Liu, C. Chang, J. Liu, X. Wu, L. Ma, and X. Qi, "Mars3d: A plug-and-play motion-aware model for semantic segmentation on multi-scan 3d point clouds," *Proc. of the IEEE/CVF Conf. on Computer Vision and Pattern Recognition (CVPR)*, pp. 9372–9381, 2023.
- [12] J. Behley, M. Garbade, A. Milioto, J. Quenzel, S. Behnke, C. Stachniss, and J. Gall, "SemanticKITTI: A Dataset for Semantic Scene Understanding of LiDAR Sequences," in *Proc. of the IEEE/CVF Intl. Conf. on Computer Vision (ICCV)*, 2019.
- [13] C. Choy, J. Gwak, and S. Savarese, "4d spatio-temporal convnets: Minkowski convolutional neural networks," in *Proc. of the IEEE/CVF Conf. on Computer Vision and Pattern Recognition (CVPR)*, 2019.
- [14] P. Schutt, R. A. Rosu, and S. Behnke, "Abstract flow for temporal semantic segmentation on the permutohedral lattice," in *Proc. of the IEEE Intl. Conf. on Robotics & Automation (ICRA)*, 2022, pp. 5139–5145.
- [15] X. Chen, S. Li, B. Mersch, L. Wiesmann, J. Gall, J. Behley, and C. Stachniss, "Moving Object Segmentation in 3D LiDAR Data: A

- Learning-based Approach Exploiting Sequential Data,” *IEEE Robotics and Automation Letters (RA-L)*, vol. 6, pp. 6529–6536, 2021.
- [16] J. Sun, Y. Dai, X. Zhang, J. Xu, R. Ai, W. Gu, and X. Chen, “Efficient spatial-temporal information fusion for lidar-based 3d moving object segmentation,” in *Proc. of the IEEE/RSJ Intl. Conf. on Intelligent Robots and Systems (IROS)*. IEEE, 2022, pp. 11 456–11 463.
- [17] X. Chen, B. Mersch, L. Nunes, R. Marcuzzi, I. Vizzo, J. Behley, and C. Stachniss, “Automatic labeling to generate training data for online lidar-based moving object segmentation,” *IEEE Robotics and Automation Letters (RA-L)*, vol. 7, no. 3, pp. 6107–6114, 2022.
- [18] S. Mohapatra, M. Hodaei, S. Yogamani, S. Milz, H. Gotzig, M. Simon, H. Rashed, and P. Maeder, “Limoseg: Real-time bird’s eye view based lidar motion segmentation,” *arXiv preprint*, 2021.
- [19] B. Zhou, J. Xie, Y. Pan, J. Wu, and C. Lu, “Motionbev: Attention-aware online lidar moving object segmentation with bird’s eye view based appearance and motion features,” *IEEE Robotics and Automation Letters (RA-L)*, vol. 8, no. 12, pp. 8074–8081, 2023.
- [20] B. Mersch, X. Chen, I. Vizzo, L. Nunes, J. Behley, and C. Stachniss, “Receding moving object segmentation in 3d lidar data using sparse 4d convolutions,” *IEEE Robotics and Automation Letters (RA-L)*, vol. 7, no. 3, pp. 7503–7510, 2022.
- [21] P. Patil, K. Biradar, A. Dudhane, and S. Murala, “An end-to-end edge aggregation network for moving object segmentation,” in *Proc. of the IEEE/CVF Conf. on Computer Vision and Pattern Recognition (CVPR)*, 2020.
- [22] J. H. Giraldo, S. Javed, and T. Bouwmans, “Graph moving object segmentation,” *IEEE Trans. on Pattern Analysis and Machine Intelligence (TPAMI)*, vol. 44, no. 5, pp. 2485–2503, 2022.
- [23] T. Kreutz, M. Mühlhäuser, and A. S. Guinea, “Unsupervised 4d lidar moving object segmentation in stationary settings with multivariate occupancy time series,” in *Proc. of the IEEE Winter Conf. on Applications of Computer Vision (WACV)*, 2023, pp. 1644–1653.
- [24] N. Wang, C. Shi, R. Guo, H. Lu, Z. Zheng, and X. Chen, “Insmos: Instance-aware moving object segmentation in lidar data,” in *Proc. of the IEEE/RSJ Intl. Conf. on Intelligent Robots and Systems (IROS)*, 2023, pp. 7598–7605.
- [25] B. Graham, M. Engelcke, and L. van der Maaten, “3D Semantic Segmentation with Submanifold Sparse Convolutional Networks,” in *Proc. of the IEEE Conf. on Computer Vision and Pattern Recognition (CVPR)*, 2018.
- [26] X. Lai, Y. Chen, F. Lu, J. Liu, and J. Jia, “Spherical transformer for lidar-based 3d recognition,” in *Proc. of the IEEE/CVF Conf. on Computer Vision and Pattern Recognition (CVPR)*, 2023, pp. 17 545–17 555.
- [27] T. Yin, X. Zhou, and P. Krahenbuhl, “Center-Based 3D Object Detection and Tracking,” in *Proc. of the IEEE/CVF Conf. on Computer Vision and Pattern Recognition (CVPR)*, 2021.
- [28] H. Li, G. Chen, G. Li, and Y. Yu, “Motion guided attention for video salient object detection,” in *Proc. of the IEEE/CVF Intl. Conf. on Computer Vision (ICCV)*, 2019, pp. 7273–7282.
- [29] S. Woo, J. Park, J. Y. Lee, and I. S. Kweon, “Cbam: Convolutional block attention module,” in *Proc. of the Europ. Conf. on Computer Vision (ECCV)*, 2018, pp. 3–19.
- [30] L. Liebel and M. Körner, “Auxiliary tasks in multi-task learning,” *arXiv preprint*, 2018.
- [31] X. Zhang, W. Xu, C. Dong, and J. M. Dolan, “Efficient l-shape fitting for vehicle detection using laser scanners,” in *2017 IEEE Intelligent Vehicles Symposium (IV)*, 2017, pp. 54–59.
- [32] A. Paszke, S. Gross, F. Massa, A. Lerer, J. Bradbury, G. Chanan, T. Killeen, Z. Lin, N. N. Gimeshain, L. Antiga, *et al.*, “PyTorch: An Imperative Style, High-Performance Deep Learning Library,” in *Proc. of the Conference on Neural Information Processing Systems (NeurIPS)*, 2019, pp. 8026–8037.
- [33] M. Everingham, L. Van Gool, C. Williams, J. Winn, and A. Zisserman, “The Pascal Visual Object Classes (VOC) Challenge,” *Intl. Journal of Computer Vision (IJCV)*, vol. 88, no. 2, pp. 303–338, 2010.